Chapter 1
Geometrically Frustrated Antiferromagnets: Statistical Mechanics and Dynamics

John T. Chalker

Abstract These lecture notes provide a simple overview of the physics of geometrically frustrated magnets. The emphasis is on classical and semiclassical treatments of the statistical mechanics and dynamics of frustrated Heisenberg models, and on the ways in which the results provide an understanding of some of the main observed properties of these systems.

1.1 Introduction

This chapter is intended to give an introduction to the theory of thermal fluctuations and their consequences for static and dynamic correlations in geometrically frustrated antiferromagnets, focusing on the semiclassical limit, and to discuss how our theoretical understanding leads to an explanation of some of the main observed properties of these systems. A central theme will be the fact that simple, classical models for highly frustrated magnets have a ground state degeneracy which is *macroscopic*, though *accidental* rather than a consequence of symmetries. We will be concerned in particular with (a) the origin of this degeneracy and the possibility that it is lifted by thermal or quantum fluctuations; (b) correlations within ground states; and (c) low-temperature dynamics. We concentrate on Heisenberg models with large spin S, referring to the Chap. 16 by G. Misguich for a discussion of quantum spin liquids, and to the Chap. 12 by M. Gingras for an overview of geometrically frustrated Ising models in the context of spin ice materials. Several earlier reviews provide useful further reading, including [1–3] for experimental background, and [4, 5] for an alternative perspective on theory.

To provide a comparison, it is useful to begin by recalling the behaviour of an *unfrustrated* antiferromagnet. To be definite, consider the Heisenberg model with nearest neighbour exchange J on a simple cubic lattice. As the lattice is bipartite – it can be separated into two interpenetrating sublattices, in such a way that sites of one sublattice have as their nearest neighbours only sites from the other sublattice – the classical ground states are two-sublattice Néel states, in which spins on one

sublattice all have the same orientation, and those on the other sublattice have the opposite orientation. These states are unique up to global spin rotations, which are a symmetry of the model. Their only low energy excitations are long wavelength spinwaves. These are Goldstone modes – a consequence of the symmetry breaking in ground states – and have a frequency $\omega(\mathbf{k})$ that is linear in wavevector $\mathbf{k}$ at small k. This classical picture carries over to the quantum system, and for $S \gg 1$ it is sufficient to take account of fluctuations using harmonic spinwave theory. In particular, within this approximation the sublattice magnetisation at low temperature is reduced from its classical ground state value S by an amount

$$\delta S = \frac{1}{\Omega} \int_{\mathrm{BZ}} \frac{zJS}{\hbar\omega(\mathbf{k})} \left[\langle n(\mathbf{k})\rangle + 1/2\right] \mathrm{d}^3\mathbf{k} - \frac{1}{2}, \tag{1.1}$$

where $\langle n(\mathbf{k})\rangle$ is a Bose factor giving the number of thermally excited spin waves at wavevector $\mathbf{k}$ and $1/2$ represents the zero-point contribution, with the integral running over the Brillouin zone of volume Ω. Fluctuations increase with temperature and the sublattice magnetisation falls to zero at the Néel temperature T_{N}. Within mean field theory $\mathrm{k_B} T_{\mathrm{N}} = zJS^2$, where z is the number of nearest neighbour sites (six on the simple cubic lattice).

A central reason for the interest in geometrically frustrated magnets is that they hold out the possibility of evading Néel order. At the simplest level, there is a tendency for frustrated systems to have many low-frequency modes, which means both that excitations are effective in reducing the ordered moment, because of the factor of $zJS/\hbar\omega(\mathbf{k})$ in (1.1), and that they are thermally populated even at low temperature. More fundamentally, we will see that frustration may lead to classical ground states of a quite different kind and suppress T_{N} to zero.

Since the term *frustration* is used in several different contexts, it is worthwhile to set out some distinctions before going further. In general terms, classical frustrated systems have Hamiltonians with competing interactions which make contributions to the energy that cannot simultaneously be minimised. The concept was originally discussed in relation to spin glasses, but these are set apart from the systems we are considering here by the fact that quenched disorder has a controlling influence on their properties. Frustration as a way of destabilising Néel order has been studied extensively in models with competing nearest neighbour and further neighbour interactions, notably the $J_1 - J_2$ model on the square lattice [6], illustrated in Fig. 1.1. The classical ground state of this model depends on the ratio J_1/J_2. For $J_1 > 2J_2 > 0$ neighbouring spins are antiparallel, enforcing ferromagnetic alignment of second neighbours and frustration of the interaction J_2. In the other regime, $2J_2 > J_1 > 0$, second neighbours are antiferromagnetically aligned at the expense of frustration of half of the J_1 interactions. Interest focuses on the point $J_1 = 2J_2$ where these alternative classical states are degenerate, and the consequences of frustration are likely to be largest. While models of this kind provide an attractive starting point for theoretical work, there are likely to be difficulties in finding experimental realisations with interaction strengths that place them close to the degeneracy point. From this perspective, the long-appreciated [7, 8] attraction of geometrically

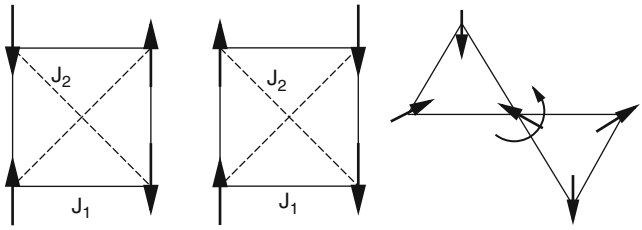

Fig. 1.1 *Left and centre*: $J_1 - J_2$ model, showing ground state spin configurations for: $2J_1 > J_2$ (*left*); and $J_2 > 2J_1$ (*centre*). *Right*: ground states of classical Heisenberg spins at vertices of two corner-sharing triangles, with degeneracy arising from rotations about the common spin, as indicated

frustrated magnets is that they are systems in which structure alone may destabilise Néel order, with only nearest neighbour interactions. To illustrate this at an elementary level, consider Heisenberg spins at the vertices of two corner-sharing triangles with nearest-neighbour antiferromagnetic interactions, also shown in Fig. 1.1. The ground states are configurations in which spins within each triangle are coplanar and at relative angles of $2\pi/3$. They have an accidental degeneracy (in addition to that arising from symmetry) under relative rotations of the spin planes for the two triangles about the axis defined by the orientation of their common spin.

1.2 Models

The models we are concerned with extend some features present in the simple system of two corner-sharing triangles to a periodic lattice. In general, we will consider non-bipartite lattices constructed from corner-sharing arrangements of frustrated clusters, with local magnetic moments at the vertices of each cluster and exchange interactions of equal strength between all moments in each cluster (other arrangements are also of interest, but typically show less dramatic consequences of frustration) [9, 10]. An important example in two dimensions is the kagomé lattice, formed from corner-sharing triangles; a three-dimensional analogue is the pyrochlore lattice, built from corner-sharing tetrahedra: see Fig. 1.2 for illustrations of both.

The Hamiltonian for these models, written in terms of the exchange energy J and the spin operators $\mathbf{S}_i$ at sites i, has the form

$$\mathcal{H} = J \sum_{\langle ij \rangle} \mathbf{S}_i \cdot \mathbf{S}_j \equiv \frac{J}{2} \sum_{\alpha} |\mathbf{L}_\alpha|^2 + c$$
$$\text{where} \quad \mathbf{L}_\alpha = \sum_{i \in \alpha} \mathbf{S}_i . \tag{1.2}$$

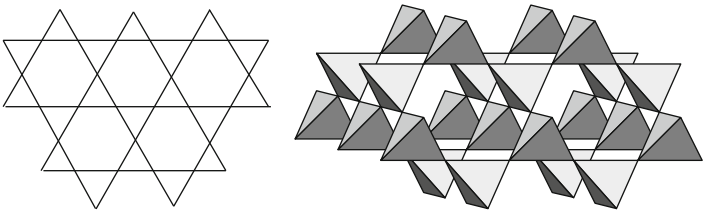

Fig. 1.2 *Left*: kagomé lattice. *Right*: pyrochlore lattice

Here, the first sum runs over neighbouring pairs ij of sites, while the second sum is over clusters α. To recognise that this second expression is a correct rewriting of $\mathcal{H}$ in terms of the total spin $\mathbf{L}_\alpha$ of each cluster α, it is necessary only to note that expansion of $|\mathbf{L}_\alpha|^2$ generates the required off-diagonal terms $\mathbf{S}_i \cdot \mathbf{S}_j$, together with diagonal terms $\mathbf{S}_i^2$ that contribute to the constant c. The apparent simplicity of this second form is of course deceptive, since the operators $\mathbf{L}_\alpha$ and $\mathbf{L}_\beta$ associated with two clusters α and β that share a site are not independent.

For future reference it is useful to introduce some terminology. The frustrated clusters are in general simplices, and their centres occupy sites of a second lattice, called the simplex lattice. Spins in our models are located at the mid-points of nearest-neighbour links of the simplex lattice. For the kagomé magnet the simplex lattice is the honeycomb lattice, and for the pyrochlore magnet it is the diamond lattice.

While the Hamiltonian of (1.2) provides a useful basis for understanding the properties of a range of geometrically frustrated magnetic materials, various additional physical contributions to a realistic model may also be important. These include single-ion anisotropy [11], further neighbour exchange [12, 13], dipolar interactions [14, 15], Dzyaloshinskii–Moriya interactions [16], magnetoelastic coupling [17], site dilution [18, 19] and exchange randomness [20]. In many cases, the associated energy scales are small. They set a temperature scale much smaller than nearest-neighbour exchange, below which they may induce magnetic order or spin freezing, but they can be neglected at higher temperatures. We omit all these perturbations and restrict our discussion to models with only nearest neighbour exchange.

1.3 Some Experimental Facts

The single most revealing property of a geometrically frustrated magnet is arguably the dependence on temperature T of its magnetic susceptibility χ. It is convenient to consider plots of χ^{-1} vs T, which at high temperature have the linear form

$$\chi^{-1} \propto T - \Theta_{\rm CW}, \tag{1.3}$$

where the Curie–Weiss constant $\Theta_{\rm CW}$ characterises the sign and strength of interactions. In an antiferromagnet $\Theta_{\rm CW}$ is negative, and for the model of (1.2) one has $k_B\Theta_{\rm CW} = -zJS^2$. Without frustration, magnetic order, signalled by a cusp in χ, appears below the Néel temperature, $T_N \sim |\Theta_{\rm CW}|$. By contrast, in geometrically frustrated systems nothing sharp is observed at the temperature scale set by interaction strength: instead, the paramagnetic phase extends to temperatures $T \ll \Theta_{\rm CW}$. Ordering or spin freezing may appear at a lower temperature T_c, but a large value for the ratio $f \equiv |\Theta_{\rm CW}|/T_c$ is a signature of frustration [1]. This behaviour is illustrated schematically in Fig. 1.3; references to experimental papers are given in Table 1.1.

More detailed information on low temperature behaviour is provided by magnetic neutron scattering (see the Chap. 3 by S.T. Bramwell). Again, we sketch typical observations in Fig. 1.3, and give references in Table 1.1. The dynamical structure factor $S(Q,\omega)$ has a broad peak at finite wavevector Q, showing that spin correlations are predominantly short-range and antiferromagnetic. The width of this peak indicates a correlation length of order the lattice spacing, while the small value of the elastic scattering cross-section for $Q \to 0$ shows that correlations suppress long wavelength fluctuations in magnetisation density. This form stands in contrast both to that in unfrustrated antiferromagnets, where Néel order leads to magnetic Bragg peaks, and to that in systems with short-range ferromagnetic correlations, where the structure factor is peaked at $Q = 0$. Inelastic scattering has a width in frequency ω that decreases with decreasing temperature, and in materials that show spin freezing, scattering weight is transferred from the inelastic to the elastic response with little change in Q-dependence on cooling through T_c.

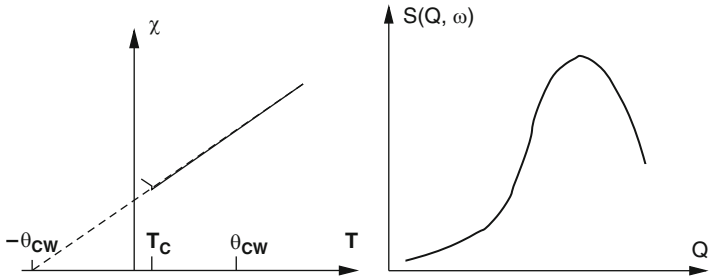

Fig. 1.3 Characteristic behaviour of a geometrically frustrated antiferromagnet. *Left*: sketch of χ^{-1} vs T. *Right*: sketch of $S(Q,\omega)$ vs Q

Table 1.1 Three geometrically frustrated antiferromagnets

Material	Structure	$\lvert\Theta_{\rm CW}\rvert$	T_c	References
$SrGa_3Cr_9O_{19}$	Pyrochlore slabs	515 K	4 K	[21–24]
Hydronium iron jarosite	Kagomé	700 K	14 K	[25]
$Y_2Mo_2O_7$	Pyrochlore	200 K	22 K	[26, 27]

Properties of three well-studied geometrically frustrated antiferromagnets are set out in Table 1.1.[1] Two basic theoretical questions arise. Why is there no magnetic ordering at $T \sim |\Theta_{\rm CW}|$? And what is the nature of correlations in the strongly interacting regime $T \ll \Theta_{\rm CW}$?

1.4 Classical Ground State Degeneracy

To get insight into the answers to these questions, we start by considering ground states of models defined by (1.2) in the classical limit, in which the $\mathbf{S}_i$ are not operators but three-component vectors of magnitude S. As a first step, it is useful to examine a single tetrahedral cluster of four spins, with the Hamiltonian

$$\mathcal{H} = \frac{J}{2}\,|\mathbf{L}|^2 + c \qquad \text{where} \qquad \mathbf{L} = \mathbf{S}_1 + \mathbf{S}_2 + \mathbf{S}_3 + \mathbf{S}_4. \tag{1.4}$$

By writing the Hamiltonian in terms of the cluster spin $\mathbf{L}$ we see at once that ground states are those with $\mathbf{L} = \mathbf{0}$. Such an arrangement of four vectors, each having three components, with resultant zero is shown in Fig. 1.4: these ground states have two internal degrees of freedom, indicated in Fig. 1.4 by the angles θ and ϕ, in addition to the degeneracies under global rotations which are expected from the symmetry of $\mathcal{H}$.

We should next understand how this accidental ground state degeneracy extends from a single cluster to a periodic lattice. We can do so using a counting argument [9, 10], which compares F, the number of degrees of freedom in the system with K, the number of constraints that must be satisfied in ground states. The central point is that if all constraints are independent, then the number of ground state degrees of freedom is given by the difference $F - K$. Such an argument was used by Maxwell in 1864 to discuss the stability of mechanical systems of jointed rods [28], and is sometimes referred to as a *Maxwellian counting argument*. For a system of $N_{\rm s}$

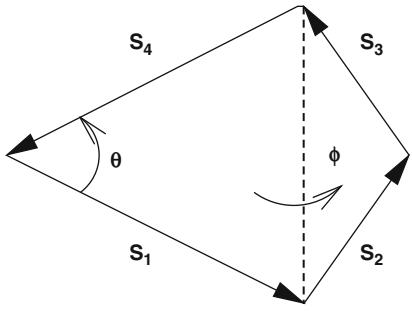

Fig. 1.4 A ground state configuration for a frustrated cluster of four classical Heisenberg spins

[1] All three examples show spin freezing below $T_{\rm c}$.

classical Heisenberg spins, $F = 2N_s$, since two angles are required to specify the orientation of each spin. And in a system with the Hamiltonian of (1.2) consisting of N_c clusters, $K = 3N_c$, since in ground states all three components of $\mathbf{L}_\alpha$ must be zero for every cluster α. Under the assumptions that all constraints can be satisfied simultaneously, and that they are all linearly independent, we arrive at an estimate for D, the number of ground-state degrees of freedom: $D = F - K$. Taking the example of the pyrochlore lattice, we have $N_s = 2N_c$ (since four spins are associated with each tetrahedron, but every spin is shared between two tetrahedra) and hence $D = N_c$, an extensive quantity.

This is a striking conclusion: it suggests that there are local degrees of freedom which can fluctuate independently without the system leaving its ground state manifold. The argument has two implications for our understanding of the experimental results summarised in Sect. 1.3. First, macroscopic degeneracy may prevent long range order at the temperature scale set by interaction strength, since there are many low-energy configurations that lack order. Second, since the magnetisation of each cluster is zero in *all* ground states, the amplitude of long wavelength fluctuations in the magnetisation density is small at low temperature, and so the dynamical structure factor $S(Q, \omega)$ is small at low Q.

At this point it is worth pausing to consider possible limitations to the counting argument that has been presented. As noted, it rests on an assumption that all ground state constraints are linearly independent. If this is not the case, we underestimate D. In our context, corrections are important if they make an extensive contribution to D. This occurs in the kagomé lattice Heisenberg antiferromagnet: in this case our estimate yields $D = 0$ (since, for a lattice built from corner-sharing triangles, $N_s = 3N_c/2$), but by explicit construction one finds sets of states with special spin arrangements [29, 30] for which $D = N_s/9$. Such an arrangement is illustrated in Fig. 1.5. By contrast, for the pyrochlore Heisenberg antiferromagnet, it is known [9, 10] that corrections to the estimate for D are at most sub-extensive.

The view of classical geometrically frustrated Heisenberg antiferromagnets that emerges at this stage is summarised by the cartoon of phase space given in Fig. 1.6:

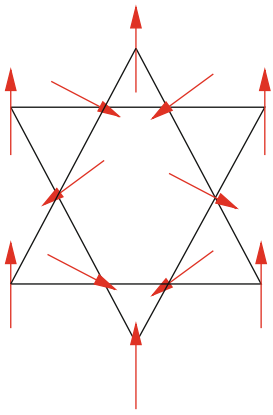

Fig. 1.5 Illustration of how ground state degrees of freedom arise for the Heisenberg model on the kagomé lattice: spins on the central hexagon may be rotated together through any angle about the axis defined by the outer spins, without leaving the ground state

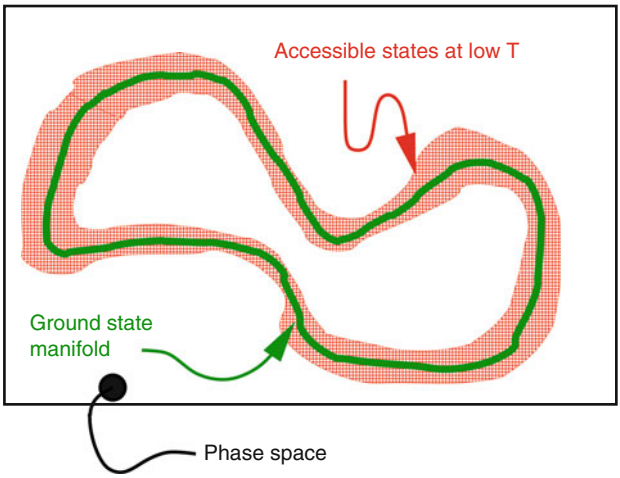

Fig. 1.6 Schematic view of phase space for a geometrically frustrated magnet

within (high-dimensional) phase space for the system as a whole, the ground states form a manifold with a dimension that is much smaller but nevertheless extensive. At temperatures small compared to the Curie–Weiss constant ($k_B T \ll JS^2$), the system is confined to a region of phase space that forms a thin layer around the ground state manifold. Quantum effects can be neglected provided $JS \ll k_B T$, and so a strongly correlated, classical window, $JS \ll k_B T \ll JS^2$, opens for large S.

1.5 Order by Disorder

The fact that extensive ground state degeneracy in classical, geometrically frustrated antiferromagnets is, in the technical sense, accidental prompts us to ask whether it has robust consequences in the presence of thermal or quantum fluctuations. Specifically, since the degeneracy is not a consequence of symmetry, one expects the spectrum of fluctuations around each ground state to be different: the possibility arises that ground states with the lowest excitation frequencies are selected, because they have the largest entropy and the smallest zero-point energy. Such an apparently paradoxical mechanism, by which fluctuations enhance order instead of suppressing it, is termed 'order-by-disorder' [31, 32].

We will consider first the effects of thermal fluctuations, and begin by discussing a cluster of four spins. Two ground states with fluctuations of contrasting types are illustrated in Fig. 1.7. For the configuration shown on the left, the total spin of the cluster has a magnitude $|\mathbf{L}|$ that varies with the departure $\delta\theta$ from the ground state as $|\mathbf{L}| \propto \delta\theta$. Since the excitation energy is proportional to $|\mathbf{L}|^2$, it has a conventional, quadratic dependence on $\delta\theta$. By contrast, for the excitation from a collinear ground state shown on the right, $|\mathbf{L}| \propto (\delta\theta)^2$: this mode is therefore soft, with an energy

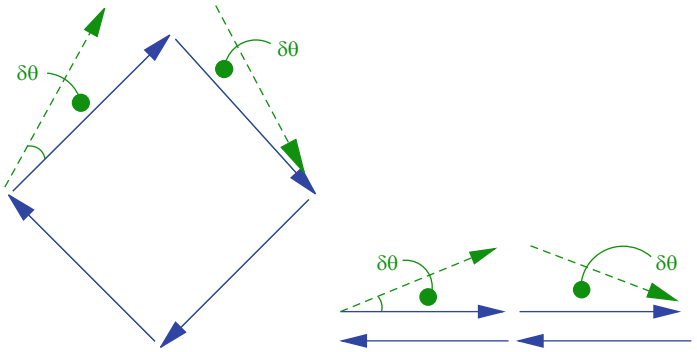

Fig. 1.7 Fluctuations away from ground state configurations for a cluster of four spins. *Left*: a conventional fluctuation; *right*: a soft mode

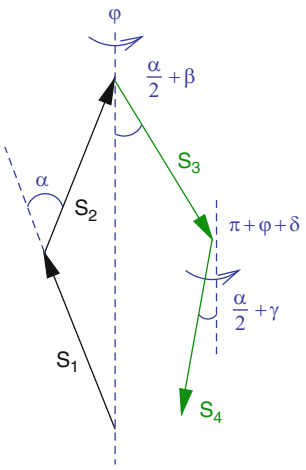

Fig. 1.8 Coordinate system used for configurations of four spins

proportional to $(\delta\theta)^4$. We wish to understand whether the presence of this soft mode leads almost collinear configurations to dominate at low temperature.

Analysis for a cluster of four spins is simple enough that it can be followed through in full. To illustrate the range of possible outcomes, we will consider spins with n components, comparing behaviour for $n = 3$ and $n = 2$. We use the coordinate system shown in Fig. 1.8. Our aim is to evaluate the thermal probability distribution $P_n(\alpha)$ of the angle α between the pair of spins $\mathbf{S}_1$ and $\mathbf{S}_2$. The distribution $P_n(\alpha)\mathrm{d}\alpha$ is a product of two factors. One stems from the measure for $\mathbf{S}_2$, and is $\sin(\alpha)\mathrm{d}\alpha$ or $\mathrm{d}\alpha$, for $n = 3$ or $n = 2$ respectively. The other comes from integrating over orientations of $\mathbf{S}_3$ and $\mathbf{S}_4$: it is

$$\mathcal{Z}_n(\alpha) \propto \int \mathrm{d}\mathbf{S}_3 \int \mathrm{d}\mathbf{S}_4 \exp\left(-\frac{J}{2T}\,|\mathbf{S}_3 + \mathbf{S}_4 - 2S\cos(\alpha/2)\hat{z}|^2\right). \qquad (1.5)$$

In the low temperature limit, this can be evaluated by expanding the energy to quadratic order in deviations from a ground state. For Heisenberg spins ($n = 3$) the low energy configurations have $|\beta|, |\gamma|, |\delta| \ll 1$; for $n = 2$, spins are coplanar and two coordinates are fixed: $\varphi = \delta = 0$. In a quadratic approximation, the energy is

$$\frac{JS^2}{2}\left\{(\beta-\gamma)^2\cos^2(\alpha/2) + \left[(\beta+\gamma)^2+\delta^2\right]\sin^2(\alpha/2)\right\}, \tag{1.6}$$

so that (including for $n = 3$ a factor of $\sin^2(\alpha/2)$ arising from $\mathrm{d}\mathbf{S}_3\mathrm{d}\mathbf{S}_4$)

$$\mathcal{Z}_3(\alpha) \propto [\cos(\alpha/2)]^{-1} \qquad \text{and} \qquad \mathcal{Z}_2 \propto [\cos(\alpha/2)\sin(\alpha/2)]^{-1}. \tag{1.7}$$

Combining contributions, we have

$$P_3(\alpha) \propto \sin(\alpha/2) \qquad \text{and} \qquad P_2(\alpha) \propto \frac{1}{\sin(\alpha)}. \tag{1.8}$$

In this way, we discover contrasting behaviour for the two cases. With $n = 3$, the system explores all values of α even in the low temperature limit. But for $n = 2$ our unnormalised result for $Z_2(\alpha)$ has non-integrable divergences at $\alpha = 0$ and $\alpha = \pi$: in a more detailed treatment, retaining contributions to the energy quartic in coordinates, these divergences are cut off on a scale set by temperature, but in the low-temperature limit $P_2(\alpha)$ approaches a sum of two delta functions, located at $\alpha = 0$ and $\alpha = \pi$. Thus, order by disorder is absent for $n = 3$ but perfect for $n = 2$.

Passing from a single cluster to an extended system, consider the sketch of phase space given in Fig. 1.9. Here, repeating the convention of Fig. 1.6, the shading

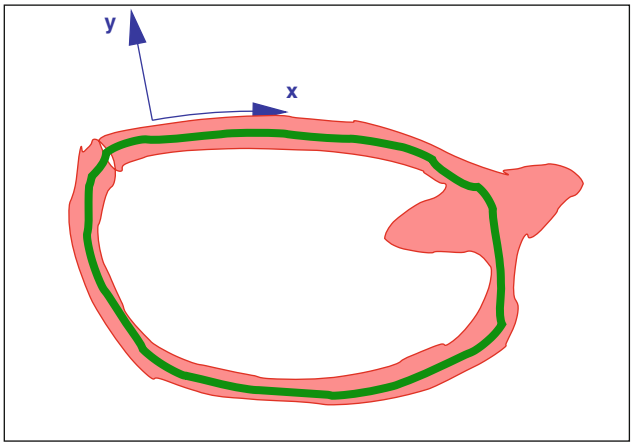

Fig. 1.9 Schematic view of phase space. The full curve represents the ground state manifold. Coordinates x and y are respectively parallel and perpendicular to it

indicates the region accessible at low temperature. One part of this region is concentrated near points on the ground state manifold at which there are soft modes, as represented by in Fig. 1.9 by a bulge, while another part is distributed in the neighbourhood of the remainder of the ground state manifold. To decide whether the system displays order by disorder, we need to understand which of these two parts dominates. Introducing coordinates $\mathbf{x}$ and $\mathbf{y}$, respectively parallel and perpendicular to the ground state manifold, in the low temperature limit we obtain a measure $P(\mathbf{x})$ on the ground state manifold by integrating over transverse fluctuations [9,10]. Characterising these fluctuations by dynamical frequencies $\omega_l(\mathbf{x})$, we obtain

$$P(\mathbf{x}) \propto \prod_l \left(\frac{\mathrm{k_B} T}{\hbar \omega_l(\mathbf{x})} \right). \tag{1.9}$$

The system has extra soft modes (in addition to those associated with the ground state coordinates $\mathbf{x}$) at points $\mathbf{x_0}$ where one or more of the harmonic frequencies $\omega_l(\mathbf{x_0})$ vanishes. At these points $P(\mathbf{x_0})$ is divergent. As for a cluster of four spins, behaviour depends on whether any such divergence is integrable. If it is, the system explores the whole of the ground state manifold in the low temperature limit, but if it is not, then those ground states with soft modes are selected by thermal fluctuations. Detailed considerations, tested using Monte Carlo simulations, show for the Heisenberg antiferromagnet on the kagomé lattice that there is coplanar spin order in the low temperature limit [29], while on the pyrochlore lattice there is no order by disorder [9, 10].

The possibility of ground state selection due to quantum fluctuations can be discussed using an approach similar in spirit to the one we have taken for thermal fluctuations, although the outcome has significant differences. Referring again to Fig. 1.9, one can treat excitations around a particular point $\mathbf{x}$ on the ground state manifold using harmonic spin wave theory. Excitations involving the coordinates $\mathbf{y}$ locally orthogonal to the ground state manifold are conventional modes with non-zero frequencies $\omega_l(\mathbf{x})$, which have already made an appearance in (1.9). By contrast, fluctuations involving the coordinates $\mathbf{x}$ are, within a harmonic approximation, zero modes. The zero-point energy of the conventional, finite-frequency modes provides an effective Hamiltonian for these remaining degrees of freedom, the classical ground state coordinates. This Hamiltonian takes the form

$$\mathcal{H}_{\mathrm{eff}}(\mathbf{x}) = \frac{1}{2} \sum_l \hbar \omega_l(\mathbf{x}). \tag{1.10}$$

The components of $\mathbf{x}$ consist of pairs that are, within the approximations of harmonic spin wave theory (see (1.14)), canonically conjugate. Treating them as classical commuting variables, the ground state is the set of points $\mathbf{x}_\mathrm{G}$ on which $\mathcal{H}_{\mathrm{eff}}(\mathbf{x})$ is minimised. More accurately, the ground state wavefunction for large S is peaked at $\mathbf{x}_\mathrm{G}$, but has zero-point fluctuations in an effective potential defined by $\mathcal{H}_{\mathrm{eff}}(\mathbf{x})$.

It is not straightforward to anticipate what features of a classical ground state spin configuration will minimise $\mathcal{H}_{\rm eff}(\mathbf{x})$: since all $\omega_l(\mathbf{x})$ contribute, one could equally imagine focusing on either the highest frequencies or the lowest ones. In the examples that have been studied in detail, however, it seems that minima lie at points $\mathbf{x}_{\rm G}$ where some $\omega_l(\mathbf{x})$ vanish, which we have seen are also the states favoured by thermal fluctuations. In particular, for Heisenberg antiferromagnets at large S the selected spin configurations are coplanar on the kagomé lattice [33] and collinear on the pyrochlore lattice [34]. In both examples, one-third of the $\omega_l(\mathbf{x})$ become soft modes at the corresponding points $\mathbf{x}_{\rm G}$: the coplanar or collinear configurations, respectively.

The principal difference between the ordering effects of thermal and quantum fluctuations is that in the first case, as we have seen, order may or may not arise on the limit $J \gg T$, depending on the nature of the thermal ground state distribution $P(\mathbf{x})$, while in the second case we always expect order for $S \gg 1$, because by taking S sufficiently large, one can ensure that quantum fluctuations around the minimum of $\mathcal{H}_{\rm eff}(\mathbf{x})$ are arbitrarily small. Within this framework, the scenario by which one arrives at a spin liquid on reducing S is clear, at least in principle. For smaller S, the quantum fluctuations are larger and the ground state wavefunction is less well localised around the minimum of $\mathcal{H}_{\rm eff}(\mathbf{x})$, while below a critical value of S, the quantum ground state wavefunction becomes delocalised over the entire classical ground state manifold and the system loses magnetic order. At large, fixed S long range order induced by quantum fluctuations is suppressed thermally above a critical temperature $T_{\rm c} \sim JS$. While the expectation that spin liquids are favoured at small S is common to our discussions of both (1.1) and (1.10), one should of course remember that the two equations embody different physics: harmonic and anharmonic fluctuations, respectively.

Efforts to identify experimental examples of order by disorder must face the problem of establishing that fluctuations, rather than additional interaction terms in the Hamiltonian, are the cause of what is observed. For the garnet $Ca_3Fe_2Ge_3O_{12}$, a material with two interpenetrating magnetic lattices coupled via zero-point fluctuations, it has been shown that a spinwave gap in the Néel ordered state indeed arises mainly in this way, by independent determination of the size of single ion anisotropy (the other possible origin for the gap) [35], and via the characteristic temperature dependence of the gap [36].

1.6 Ground State Correlations

As we have seen, in some circumstance a model geometrically frustrated magnet (for example, the classical Heisenberg model on the pyrochlore lattice) explores its entire ground state manifold at low temperature, and the experimental evidence from elastic and inelastic neutron scattering suggests that this is a reasonable picture for the behaviour of a range of frustrated magnetic materials. We are led to ask in this section whether there are any important correlations within the ground state manifold. We will find (for a large class of models: those in which the simplex lattice is

bipartite) that there are indeed long-range correlations within ground states [10], and that these can be characterised in terms of fluctuations of a Gaussian, divergenceless field [37,38]. For this reason, the set of ground states is said to constitute a Coulomb phase.

The possibility that spin correlations, averaged over ground states, have a long-range component, is not self-evident. Indeed, one might expect the fact that there are a macroscopic number of ground state degrees of freedom to signal the opposite, since their existence implies that the set of ground states includes local degrees of freedom that can fluctuate independently. In turns out, however, that some ground state correlations are impervious to all local fluctuations: in this sense they can be said to be topological.

The simplest way to appreciate the existence of long-range correlations within ground states is to start from (1.2) and the fact that the total spin $\mathbf{L}_\alpha$ of each frustrated cluster α vanishes within all ground states. A consequence of this on the pyrochlore lattice can be visualised with reference to Fig. 1.2. In particular, consider for any ground state the total magnetisation $\mathbf{m}(z)$ of the lowest plane of sites in this figure. Its value (which may be small – for example, of order the square root of the number of sites within the plane, if spins are randomly orientated within the layer) is perfectly correlated with the magnetisation of other parallel planes making up the lattice. Indeed, let $\mathbf{m}(z+1)$ be the magnetisation of the plane neighbouring the lowest one. Since the sites in both planes taken together make up a layer of complete tetrahedra, the overall magnetisation of the layer is zero, and so $\mathbf{m}(z+1) = -\mathbf{m}(z)$. By extension, $\mathbf{m}(z+n) = (-1)^n \times \mathbf{m}(z)$ for any n, a signal of long range correlations. The correlations give rise to sharp features, termed *pinch points* or *bow ties* in the Fourier transform of the two-point correlation function, averaged over ground states, as obtained from simulations [39], large-n calculations [40], and diffuse neutron scattering measurements [41]. These singularities distinguish the diffraction pattern of the frustrated system from that of a paramagnet, but are weaker than those of Bragg peaks arising from Néel order. While their structure can be understood by building on our discussion of $\mathbf{m}(z)$ [10], a more complete approach uses a long-wavelength description of ground states.

This continuum description of the Coulomb phase is obtained by mapping spin configurations onto configurations of vector fields in such a way that the ground state condition $\mathbf{L}_\alpha = \mathbf{0}$, involving the specifics of the lattice structure, is translated into the requirement that the vector fields have lattice divergence zero. This second version of the constraint has the advantage that it can be implemented in the continuum [37, 38]. To describe the mapping in detail, it is necessary first to discuss some features of the simplex lattice, introduced in Sect. 1.2. We require the simplex lattice to be bipartite. This is the case, for example, for the diamond lattice, the simplex lattice associated with the pyrochlore lattice. (In models without a bipartite simplex lattice, the correlations discussed in this section are absent [42].) For a bipartite simplex lattice, one can adopt an orientation convention for links, taking them to be directed from the simplices of one sublattice to those of the other. In this way one can define unit vectors $\hat{e}_i$ oriented according to the convention and placed at the mid-points of links of the simplex lattice, which are also the locations of spins.

Considering in the first instance Ising spins, a spin configuration is represented as a vector field $\mathbf{B}(\mathbf{r})$ on the lattice via

$$\mathbf{B}(\mathbf{r}_i) = S_i \hat{e}_i \,. \tag{1.11}$$

The condition satisfied in ground states, $\sum_{i\in\alpha} S_i = 0$, fixes the lattice divergence of $\mathbf{B}(\mathbf{r})$ to be zero. More generally, for n-component spins $\mathbf{S}_i$ we require n flavours of vector field $\mathbf{B}^l(\mathbf{r})$, with $l = 1, 2 \ldots n$. These are related to spin components S_i^l via $\mathbf{B}^l(\mathbf{r}) = S_i^l \hat{e}_i$, so that in ground states each flavour has divergence zero. Note that the fields $\mathbf{B}^l(\mathbf{r})$ are defined in real space, and that the global O(n) symmetry of the spin Hamiltonian is implemented as a transformation within the space of flavours, l.

Continuum versions of these vector fields $\mathbf{B}^l(\mathbf{r})$ result from coarse-graining and the restriction to ground state configurations is imposed exactly by requiring the continuum fields to be solenoidal. Each coarse-grained state represents many microscopic configurations and should have an entropic weight that reflects this. It is plausible that small continuum field strengths will arise from many different microscopic configurations, and that large field strengths will be generated by fewer microscopic states. This suggests [37, 42] the weight

$$P[\mathbf{B}^l(\mathbf{r})] \propto \exp\left(-\frac{\kappa}{2}\int \mathrm{d}^d\mathbf{r} \sum_l |\mathbf{B}^l(\mathbf{r})|^2\right). \tag{1.12}$$

This theory has a single parameter, the stiffness κ, whose value affects the amplitude but not the form of correlations and is determined microscopically. In $d = 3$ dimensions all other terms consistent with symmetry that might be added to the effective action are irrelevant in the scaling sense, and so (1.12) is expected to have a universal validity. The resulting correlation function,

$$\langle B_i^l(\mathbf{0}) B_j^m(\mathbf{r})\rangle = \frac{\delta_{lm}}{4\pi\kappa}\left(\frac{3r_i r_j - r^2\delta_{ij}}{r^5}\right), \tag{1.13}$$

falls off with a fixed, integer power of distance, and has a characteristic, dipolar angle dependence.

The fixed, integer power appearing in (1.13) stands in contrast to behaviour in two other situations in statistical mechanics for which power-law correlations appear: those of a system undergoing a continuous phase transition, and of the low-temperature phase in the xy model. The form of correlations in (1.13) is instead similar to those generated by Goldstone modes in the ordered phase of a system with a spontaneously broken continuous symmetry, and an equivalence between that and the Coulomb phase can be developed by passing to a dual description of the frustrated magnet [43].

At finite temperature thermal fluctuations out of the ground state manifold generate a finite correlation length ξ which acts as a cut-off for the power-law in (1.13).

The scale ξ diverges at low temperature, as $\xi \sim T^{-1/2}$ in a Heisenberg model, and exponentially in an Ising model.

1.7 Dynamics

As we have seen in some detail, geometrically frustrated magnets in the temperature window $T_c \ll T \ll T_{CW}$ are strongly correlated, yet lack long range order. Their dynamics in this regime has novel features which we summarise in this section.

An obvious first step to understanding low temperature dynamics is to apply harmonic spinwave theory, starting from one of the ground states. The results one expects are summarised in terms of the density of states $\rho(\omega)$ in frequency ω in Fig. 1.10. Within the harmonic approximation, excitations are of two types. One type, similar to those in conventional magnets, forms a band of finite-frequency states, with a maximum frequency $\sim \mathcal{O}(JS/\hbar)$. The other type (those associated with the ground state coordinates $\mathbf{x}$, in the discussion of (1.10)) are zero modes. For example, for excitations from a generic ground state of the Heisenberg antiferromagnet on the pyrochlore lattice, one quarter are zero modes.

There is a clear interest in understanding in more detail the nature of these zero modes. In the most cases, however there is a obstacle to a simple, analytical treatment, which stems from the fact that spin configurations in representative classical ground states do not have long range order. This means that, even though the lattice itself is periodic, the equations of motion cannot be diagonalised by Fourier transform, and results of the kind sketched in Fig. 1.10 can be obtained only numerically.

To circumvent this difficulty and illustrate in a simple fashion how a dispersionless band of modes can arise, it is interesting to consider a geometrically frustrated Heisenberg antiferromagnet in the presence of a magnetic field h strong enough that

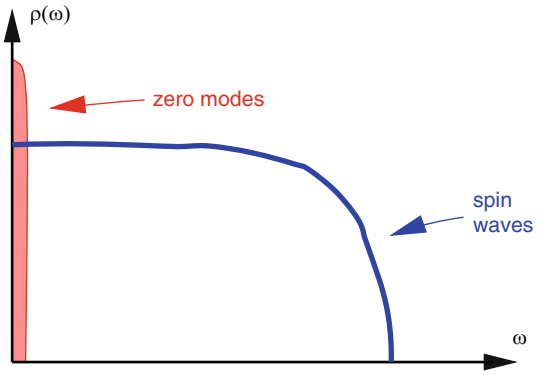

Fig. 1.10 Density of states in frequency for harmonic excitations in a geometrically frustrated antiferromagnet

the ground state is fully polarised. Using the standard Holstein–Primakoff transformation to write operators for spin components S_i^l in terms of boson creation and annihilation operators $a_i^\dagger$ and a_i, with

$$\begin{aligned} S_i^z &= S - a_i^\dagger a_i \\ S_i^+ &= (2S)^{1/2} a_i + \ldots \\ S_i^- &= (2S)^{1/2} a_i^\dagger + \ldots, \end{aligned} \tag{1.14}$$

we have

$$\mathcal{H} = J \sum_{ij} \mathbf{S}_i \cdot \mathbf{S}_j - h \sum_i S_i^z = JS \sum_{ij} \left[a_i^\dagger a_j + a_j^\dagger a_i \right] - \mu \sum_i a_i^\dagger a_i + \mathcal{O}(S^0). \tag{1.15}$$

The right-hand form of (1.15) is a tight-binding model for bosons moving on the lattice with a nearest-neighbour hopping amplitude JS and a chemical potential $\mu \equiv zJS - h$ that is linear in the magnetic field h. It is a characteristic of the lattices we are concerned with that such a tight-binding model has a dispersionless band with eigenvalue $-2JS$, which lies at the bottom of the spectrum for $J > 0$.

Eigenvectors of the tight-binding Hamiltonian from the dispersionless band are straightforward to picture. One for the kagomé lattice is represented in Fig. 1.11. Here, eigenvector amplitudes are zero at all sites except for those around one hexagon of the lattice, on which they have equal magnitude and alternating signs. The state is an eigenvector because there is destructive interference between hopping processes that move the boson off the occupied hexagon. It belongs to a dispersionless band since it is degenerate with many other, equivalent states, based on the other hexagons of the lattice. The condition for an arbitrary vector, with site amplitudes ψ_i, to be a linear superposition of such states is that $\sum_{i \in \alpha} \psi_i = 0$ for each triangle α. Both the extension of this condition to other lattices constructed from corner-sharing simplices and its parallel with the ground state condition in

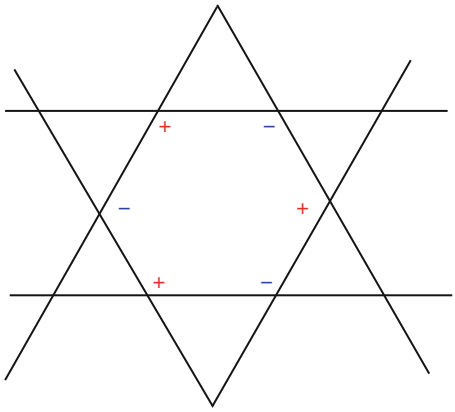

Fig. 1.11 A magnon mode from the dispersionless band

spin models, $\mathbf{L}_\alpha = \mathbf{0}$ for all α, are obvious. There is a gap to excitations for large h, when μ is large and negative. The gap falls to zero at the critical field strength $h_c = JS(z+2)$ at which μ crosses the energy of the dispersionless magnon band. For $h < h_c$ these states are populated, and the magnetisation deviates from its saturated value. In this field range we recover the classical ground state degeneracy of the zero-field problem.

We now turn to a discussion of dynamics beyond the harmonic approximation. As a starting point we should consider the full equation of motion

$$\hbar \frac{\mathrm{d}\mathbf{S}_i}{\mathrm{d}t} = \mathbf{S}_i \times \mathbf{H}_i = \frac{J}{2} \left\{ \left[\mathbf{L}_\alpha + \mathbf{L}_\beta \right] \times \mathbf{S}_i - \mathbf{S}_i \times \left[\mathbf{L}_\alpha + \mathbf{L}_\beta \right] \right\}. \tag{1.16}$$

Here $\mathbf{H}_i$ is the exchange field acting at site i. It is parallel to $\mathbf{S}_i$ in a classical ground state, but in excited states has transverse components. These can be expressed as shown, in terms of the total magnetisations $\mathbf{L}_\alpha$ and $\mathbf{L}_\beta$ of the clusters α and β that share the site i. For large S we can treat this equation of motion classically. Within the harmonic approximation, obtained by linearising the right-hand side, the exchange field $\mathbf{H}_i$ is a superposition of contributions from finite frequency modes, which maintain phase coherence indefinitely, and therefore average to zero over long times. Anharmonic interactions have two consequences, which are distinct but turn out to be closely linked [9, 10]. One is to generate a lifetime for the finite frequency modes. The other is to introduce coupling between the ground state coordinates $\mathbf{x}$ and the coordinates $\mathbf{y}$ orthogonal to the ground state manifold. Over long timescales this coupling drives the system around the ground state manifold. Within the framework of (1.16), this long-time component to the dynamics arises because, once spinwaves have a finite lifetime, the exchange field is no longer a superposition of exactly harmonic contributions. Instead, on timescales longer than the lifetime, it is better thought of as a stochastic quantity. In turn, the long-time motion of the system around the ground state manifold is itself a source of dephasing for finite frequency excitations. Specifically, since the harmonic Hamiltonian is time-dependent, an adiabatic approximation is not exact, and modes are mixed at long times. There is a separation of timescales, since typical spinwave periods are fixed, while spinwave lifetimes diverge as $T^{-1/2}$ and the timescale for motion between groundstates diverges faster, as T^{-1} [10].

These ideas suggest a much simpler approach to calculating the spin autocorrelation function, in which we treat the exchange field as a stochastic quantity, using the equation of motion

$$\frac{\mathrm{d}\mathbf{S}(t)}{\mathrm{d}t} = \mathbf{S}(t) \times \mathbf{H}(t) \tag{1.17}$$

with the correlation function

$$\langle H^l(t) H^m(t') \rangle = \Gamma \delta_{lm} \delta(t - t') \tag{1.18}$$

for components $H^l(t)$ of $\mathbf{H}(t)$. The noise intensity Γ can be estimated using equipartition. We have

$$\Gamma = \int_{-\infty}^{\infty} \langle \mathbf{H}_i(0) \cdot \mathbf{H}_i(t) \rangle \, \mathrm{d}t \sim \int_{-\infty}^{\infty} \langle \mathbf{L}_\alpha(0) \cdot \mathbf{L}_\alpha(t) \rangle \, \mathrm{d}t. \tag{1.19}$$

In addition, $\mathbf{L}_\alpha(t)$ is a superposition of contributions with amplitudes A_ω from thermally excited spinwaves:

$$\mathbf{L}_\alpha(t) = \sum_l A_{\omega_l} \mathrm{e}^{-\mathrm{i}\omega_l t}. \tag{1.20}$$

Combining these assumptions, we find [10]

$$\Gamma \sim \langle |A_\omega|^2 \rangle \rho(\omega)\big|_{\omega \to 0} \sim \frac{k_\mathrm{B} T}{JS}. \tag{1.21}$$

The Langevin equation (1.18) itself is straightforward to solve, and yields

$$\langle \mathbf{S}(0) \cdot \mathbf{S}(t) \rangle = S(S+1) \exp(-c k_\mathrm{B} T t / \hbar S), \tag{1.22}$$

where $c \sim \mathcal{O}(1)$ is an undetermined numerical constant. This result is notable for the fact that temperature alone sets the time scale: J drops out of the long-time dynamics in the low temperature regime. In this sense, behaviour matches that expected at a quantum critical point, although the underlying physics is quite different.

The predictions of (1.22) have been tested both in simulations and in experiment. Molecular dynamics simulations proceed by direct integration of the equations of motion, (1.16), with an initial configuration drawn from a thermal distribution and generated via Monte Carlo simulation. Results for the classical pyrochlore Heisenberg antiferromagnet [9, 10] in the temperature range $\mathrm{k_B} T \ll JS^2$ reproduce both the functional form of (1.22) for the time dependence of the autocorrelation function and the scaling of relaxation rate with temperature. In experiment, inelastic neutron scattering offers direct access to spin dynamics. Early measurements of the energy width of quasielastic scattering in $CsNiFe_6$ [44] were fitted to a Lorentzian, the transform of the time-dependence given in (1.22), yielding a relaxation rate for $T < |\Theta_\mathrm{CW}|$ that is strongly temperature dependent, although without specific evidence for the (subsequently proposed) linear variation with T. More detailed data for SCGO ([45]; Lee et al. unpublished) confirms a relaxation rate of order $k_\mathrm{B} T/\hbar$, and very recent measurements on $Y_2Ru_2O_7$ [46] display rather clearly a relaxation rate proportional to temperature.

Recent theoretical work [47] has mapped out the low temperature dynamics as a function of wavevector throughout the Brillouin zone.

1.8 Final Remarks

In conclusion, we have seen how geometrical frustration in classical magnets can lead to macroscopic ground state degeneracy and the suppression of long range order. Low temperature states in model systems, although disordered, are very different from those of a non-interacting paramagnet: correlations are power-law in space, and decay in time at a rate set by temperature alone. Many experimental systems display these features within the temperature window $T_c < T < |\Theta_{CW}|$ where behaviour is dominated by nearest neighbour exchange. Behaviour in this regime is well summed up in the term coined by Jacques Villain [8], a pioneer in the field: *Cooperative Paramagnetism*.

Acknowledgements

I am very grateful to my collaborators in the research on geometrically frustrated antiferromagnets that I have been involved with, especially E.F. Shender, P.C.W. Holdsworth and R. Moessner, and also J.F.G. Eastmond, S.E. Palmer, P. Hogan, M.Y. Veillette, R. Coldea, T.E. Saunders, M.J. Bhaseen and T.S. Pickles. In addition, I have benefitted from discussions with many other colleagues. I thank EPSRC for supporting this work.

References

1. A.P. Ramirez, Annu. Rev. Mater. Sci. **24**, 453 (1994)
2. P. Schiffer, A.P. Ramirez, Comments Cond. Mat. Phys. **18**, 21 (1996)
3. M.J. Harris, M.P. Zinkin, Mod. Phys. Lett. B**10**, 417 (1996)
4. R. Moessner, Can. J. Phys. **79**, 1283 (2001)
5. C.L. Henley, Can. J. Phys. **79**, 1307 (2001)
6. P. Chandra, B. Doucot, Phys. Rev. B **38**, 9335 (1988)
7. P.W. Anderson, Phys. Rev. **102**, 1008 (1956)
8. J. Villain, Z. Phys. B **33**, 31 (1979)
9. R. Moessner, J.T. Chalker, Phys. Rev. Lett. **80**, 2929 (1998)
10. R. Moessner, J.T. Chalker, Phys. Rev. B **58**, 12049 (1998)
11. M. Harris, S.T. Bramwell, D.F. McMorrow, T. Zeiske, K.W. Godfrey, Phys. Rev. Lett. **79**, 2554 (1997)
12. J.N. Reimers, A.J. Berlinsky, A.-C. Shi, Phys. Rev. B **43**, 865 (1991)
13. J.N. Reimers, J.E. Greedan, M. Björgvinsson, Phys. Rev. B **45**, 7295 (1991)
14. N. Raju, M. Dion, M.J.P. Gingras, T.E. Mason, J.E. Greedon, Phys. Rev. B **59**, 14489 (1999)
15. S.E. Palmer, J.T. Chalker, Phys. Rev. B **62**, 488 (2000)
16. M. Elhajal, B. Canals, R. Sunyer, C. Lacriox, Phys. Rev. B **71**, 94420 (2005)
17. O. Tchernyshyov, R. Moessner, S.L. Sondhi, Phys. Rev. B **66**, 64403 (2002)
18. E.F. Shender, V.B. Cherepanov, P.C.W. Holdsworth, A.J. Berlinsky, Phys. Rev. Lett. **70**, 3812 (1993)
19. R. Moessner, A.J. Berlinsky, Phys. Rev. Lett. **83**, 3293 (1999)
20. T.E. Saunders, J.T. Chalker, Phys. Rev. Lett. **98**, 157201 (2007)
21. A.P. Ramirez, G.P. Espinoza, A.S. Cooper, Phys. Rev. Lett. **64**, 2070 (1990)

22. C. Broholm, G. Aeppli, G.P. Espinosa, A.S. Cooper, Phys. Rev. Lett. **65**, 3173 (1990)
23. B. Martinez, F. Sandiumenge, A. Rouco, A. Labarta, J. Rodriguez-Cavajal, M. Tovar, M.T. Causa, S. Gali, X. Obradors, Phys. Rev. B **46**, 10786 (1992)
24. S.H. Lee, C. Brohlom, G. Aeppli, A. Ramirez, T.G. Perring, C.J. Carlile, M. Adams, T.L. Jones, B. Hessen, Europhys. Lett. **35**, 127 (1996)
25. A.S. Wills, A. Harrison, S.A.M. Menthink, T.E. Mason, Z. Tun, Europhys. Lett. **42**, 325 (1998)
26. M.J.P. Gingras, C.V. Stager, N.P. Raju, B.D. Gaulin, J.E. Greedan, Phys. Rev. Lett. **78**, 947 (1997)
27. J.S. Gardner, B.D. Gaulin, S.-H. Lee, C. Broholm, N.P. Raju, J.E. Greedan, Phys. Rev. Lett. **83**, 211 (1999)
28. J.C. Maxwell, Philos. Mag. **27**, 294 (1864)
29. J.T. Chalker, P.C.W. Holdsworth, E.F. Shender, Phys. Rev. Lett. **68**, 855 (1992)
30. I. Ritchey, P. Chandra, P. Coleman, Phys. Rev. **47**, 15342 (1993)
31. J. Villain, R. Bidaux, J.P. Carton, R.J. Conte, J. Phys. Paris **41**, 1263 (1980)
32. E.F. Shender, Sov. Phys. JETP **56**, 178 (1982)
33. A.V. Chubukov, Phys. Rev. Lett. **69**, 832 (1992)
34. C.L. Henley, Phys. Rev. Lett. **96**, 47201 (2006)
35. A.G. Gukasov, T. Brückel, B. Dorner, V.P. Plakhty, W. Prandtl, E.F. Shender, O.P. Smirnov, Europhys. Lett. **7**, 83 (1988)
36. T. Brückel, B. Dorner, A.G. Gukasov, V.P. Plakhty, Phys. Lett. A **162**, 357 (1992)
37. S.V. Isakov, K. Gregor, R. Moessner, S.L. Sondhi, Phys. Rev. Lett. **93**, 167204 (2004)
38. C.L. Henley, Phys. Rev. B **71**, 014424 (2005)
39. M. Zinkin, M.J. Harris, T. Zeiske, Phys. Rev. B **56**, 11786 (1997)
40. B. Canals, D. Garanin, Can. J. Phys. **79**, 1323 (2001)
41. T. Fennell, S.T. Bramwell, D.F. McMorrow, P. Manuel, Nat. Phys. **3**, 566 (2007)
42. D.A. Huse, W. Krauth, R. Moessner, S.L Sondhi, Phys. Rev. Lett. **91**, 167004 (2003)
43. L. Jaubert, J.T. Chalker, P.C.W. Holdsworth, R. Moessner, Phys. Rev. Lett. **100**, 067207 (2008)
44. M.J. Harris, M.P. Zinkin, T. Zeiske, Phys. Rev. B **52**, R707 (1995)
45. S.-H. Lee, Ph.D. thesis, Johns Hopkins University (1996)
46. J. van Duijn, N. Hur, J.W. Taylor, Y. Qiu, Q.Z. Huang, S.-W. Cheong, C. Broholm, T.G. Perring, arXiv:0707.2678 (2007)
47. P. Conlon, J.T. Chalker, Phys. Rev. Lett. **102**, 237106 (2009)